Electronic Supplementary Information (ESI)

Ultralong lifespan of SuperRedox Capacitor using Ti-doped $Li_3V_2(PO_4)_3$ cathode with suppressed vanadium dissolution

Yuta Harada[a] *, Naohisa Okita*[a] **, Masahiro Fukuyama*[a], *Etsuro Iwama*[a,b,c], *Wako Naoi*[d], *and Katsuhiko Naoi*[a,b,c] ***

[a] Department of Applied Chemistry, Tokyo University of Agriculture & Technology, 2-24-16 Naka-cho, Koganei, Tokyo 184-8558, Japan

[b] Global Innovation Research Organization, Tokyo University of Agriculture & Technology, 2-24-16 Naka-cho, Koganei, Tokyo, 184-8588 Japan

[c] Advanced Capacitor Research Center, Tokyo University of Agriculture & Technology, 2-24-16 Naka-cho, Koganei, Tokyo 184-8558, Japan

[d] Division of Art and Innovative Technologies, K & W Inc., 1-3-16-901 Higashi, Kunitachi, Tokyo 186-0002, Japan

* Corresponding Authors: n-okita@go.tuat.ac.jp/ k-naoi@cc.tuat.ac.jp

Thermogravimetry (TG) analyses of LVP and M(Ti, Al, and Mn)-doped LVP/MWCNT composites

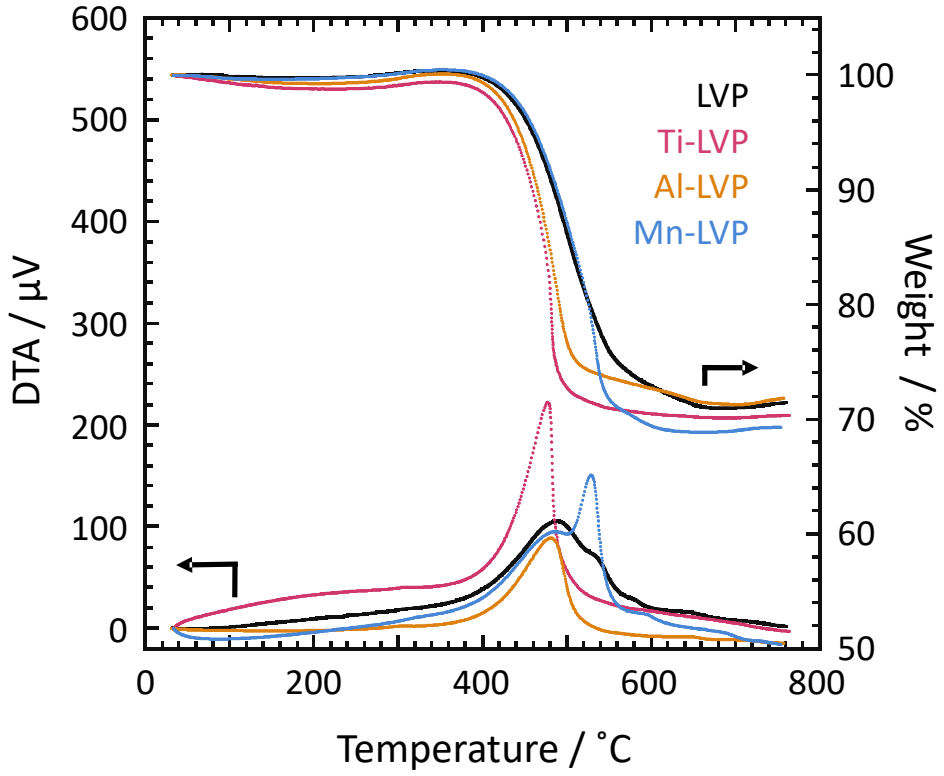

Figure S1. TG thermograms of the LVP, Ti-LVP, Al-LVP and Mn-LVP. The measurements were performed at a sweep rate of 5°C min^{-1} from ambient temperature to 750°C under a synthetic air atmosphere.

Lattice parameters of LVP/MWCNT composites (LVP, Ti-LVP, Al-LVP, and Mn-LVP)

Table S1. The lattice parameters (a, b, c, and V) of LVP/MWCNT composites (LVP, Ti-LVP, Al-LVP, and Mn-LVP). Lattice parameters were calculated by Rietveld refinement.

	a	b	c	β	V	R_{wp}
LVP	8.5935(15)	8.6105(14)	12.068(2)	90.399(14)	893.0(3)	12.91
Ti-LVP	8.5963(7)	8.6195(7)	12.0573(11)	89.594(4)	893.38(12)	11.26
Al-LVP	8.5769(16)	8.5862(15)	12.036(2)	90.309(12)	886.4(3)	11.79
Mn-LVP	8.592(2)	8.6164(19)	12.083(3)	90.312(15)	894.5(4)	7.61

Charge and discharge behaviour of $Li_3V_2(PO_4)_3$

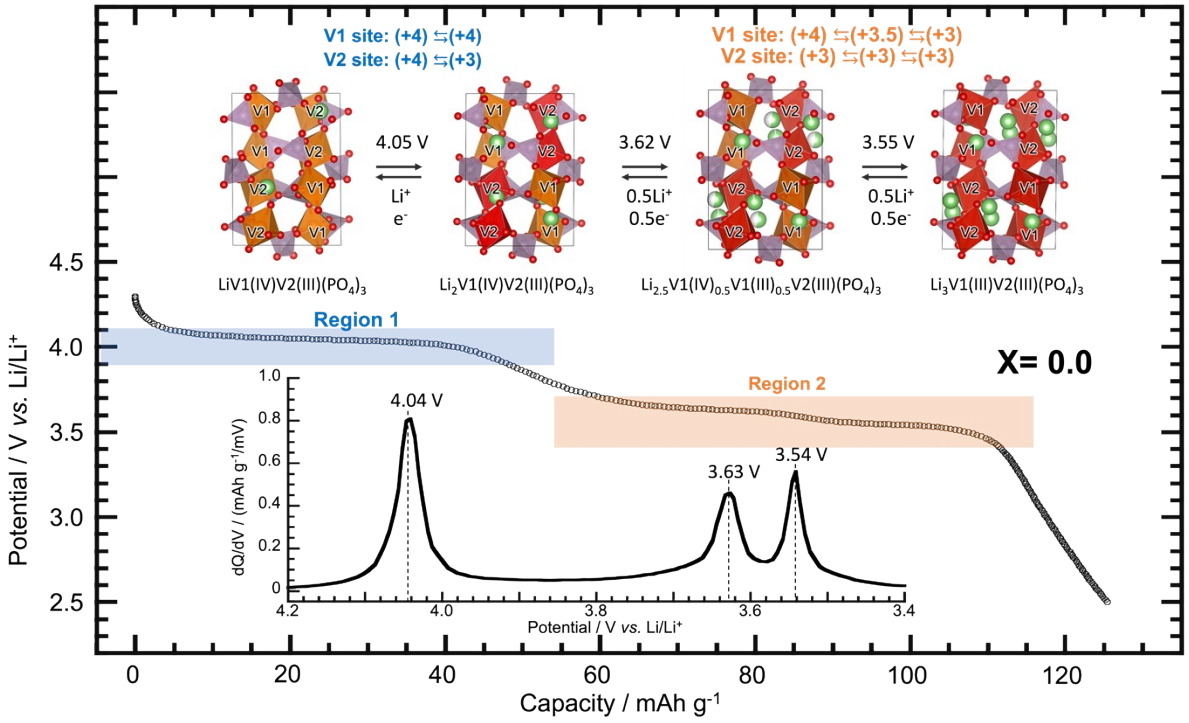

Figure S2. [confirmation with previous works] The potentials at which each phase shift have been characterized by dQ/dV vs. potential plot shown in the inlet. There observed three peaks at 4.04, 3.63, and 3.54 V. In Region 1, the redox with $1e^-/1Li^+$ occurs around 4.05V, while in Region 2, two consecutive redox reactions with each $0.5e^-/0.5Li^+$ occur. The behavior is well consistent with the admitted LVP mechanism that have been previously reported.[1] Postulated crystal structure and their transition for the of pristine(Ti-unsubstituted: X=0) $Li_3V_2(PO_4)_3$ during discharge are described with multiple/stepwise electron and Li^+ transport.

Refined structural parameters of $Li_{2.9}V_{1.9}Ti_{0.1}(PO_4)_3$

Table S2. Summary of neutron diffraction data for $Li_{2.9}V_{1.9}Ti_{0.1}(PO_4)_3$ and its Rietveld refinement.

space group	*a* / Å	*b* / Å	*c* / Å	*V* / Å^3	
$P2_1/n$	8.5961(13)	8.6130(13)	12.0393(2)	891.3508	
	x/a	*y/b*	*z/c*	B_{iso}	Occupancy
Li(1)	0.2845(11)	0.3016(11)	0.3267(9)	0.2068(3)	1.0000(3)
Li(2)	0.5606(13)	0.4169(14)	0.1857(9)	0.5396(3)	0.9092(3)
Li(3)	0.9183(12)	0.3092(11)	0.2334(8)	0.2237(2)	1.0000(3)
O(1)	0.4262(4)	0.0934(4)	0.3331(3)	0.3892(7)	1
O(2)	0.9266(4)	0.1069(5)	0.1446(3)	0.8878(8)	1
O(3)	0.3512(4)	0.4854(4)	0.2618(3)	0.5226(7)	1
O(4)	0.8025(4)	0.4996(4)	0.2177(3)	0.4428(7)	1
O(5)	0.1725(5)	0.0494(4)	0.0430(3)	0.4983(7)	1
O(6)	0.6465(5)	0.0804(4)	0.4739(3)	0.8156(8)	1
O(7)	0.4449(4)	0.3613(5)	0.0655(3)	0.5511(7)	1
O(8)	0.9286(4)	0.3269(4)	0.4092(3)	0.2321(6)	1
O(9)	0.1649(4)	0.1671(4)	0.4299(3)	0.4378(7)	1
O(10)	0.6137(4)	0.1354(5)	0.0745(3)	0.6825(8)	1
O(11)	0.1673(4)	0.2684(5)	0.1852(3)	0.7682(8)	1
O(12)	0.6411(4)	0.2937(5)	0.3219(3)	0.6973(7)	1
P(1)	0.1111(5)	0.0989(6)	0.1478(4)	0.5824(8)	1
P(2)	0.6029(5)	0.1153(5)	0.3519(3)	0.5828(7)	1
P(3)	0.0343(4)	0.2477(6)	0.4914(4)	0.2898(7)	1
V(1)	0.2461	0.4606	0.1072	0.5	0.9
V(2)	0.7534	0.4703	0.3943	0.5	1
Ti	0.2461	0.4606	0.1072	0.5	0.1

$R_{wp} = 5.35$, $R_p = 3.94$, $R_e = 1.45$, $X^2 = 3.69$

Charge and discharge behavior of $Li_{3-x}V_{2-x}Ti_x(PO_4)_3$

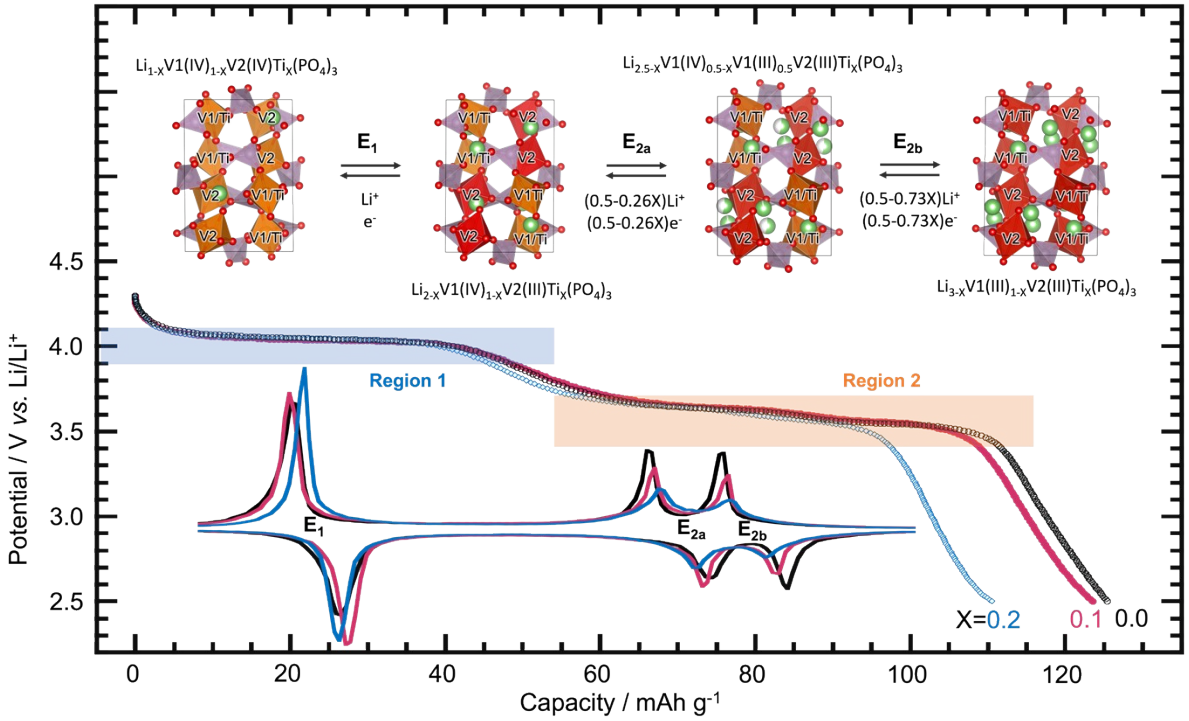

Figure S3. The same discharge curves (as in Fig.4) and their corresponding dQ/dV plots are shown, where three redox couples at around the potentials of E_{R1}, E_{R2a}, and E_{R2b} are observed. Focusing on the region 2 potential, the intensities decrease by X for the two peaks around E_{R2a} and E_{R2b}. This instantly corresponds the decrease in capacity in the discharge curves. Based on previously reported literature [1], a proposed $Li_{3-x}V_{2-x}Ti_x(PO_4)_3$ mechanism is suggested for better understanding the multiple redox with consecutive phase transition composed of two different vanadium sites (V1 and V2).

TEM images of $Li_3V_2(PO_4)_3$/MWCNT and $Li_{2.9}V_{1.9}Ti_{0.1}(PO_4)_3$/MWCNT before and after immersion in hot water.

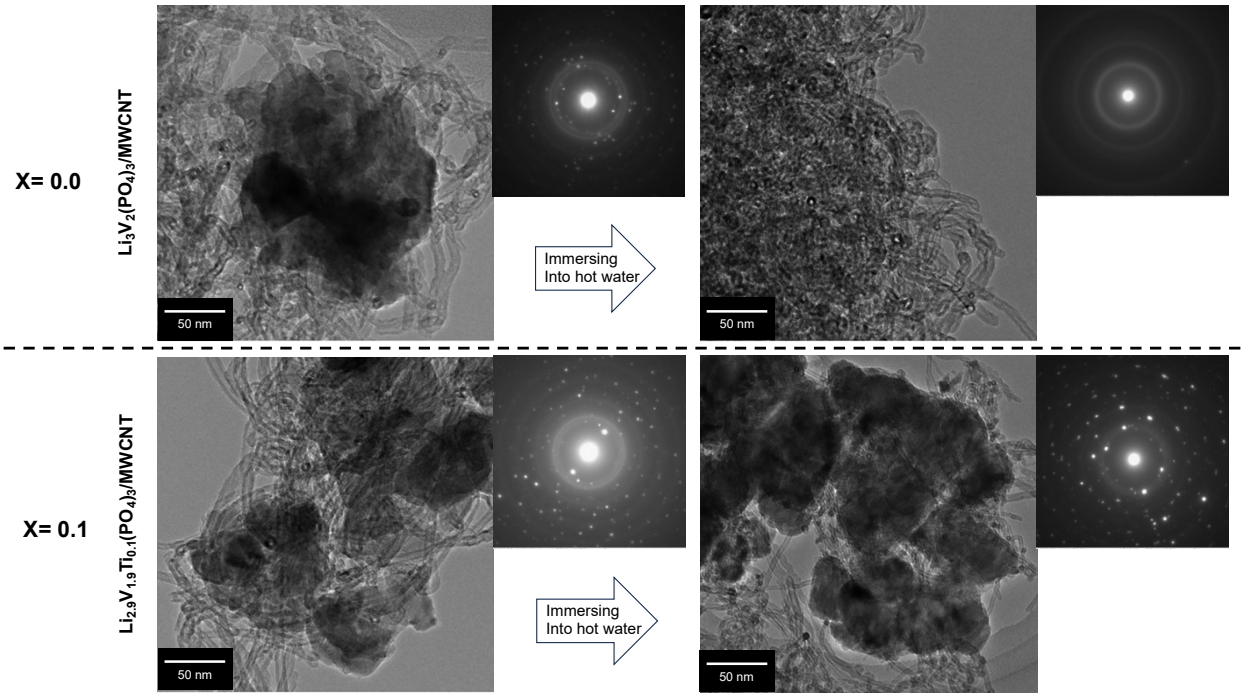

Figure S4. TEM images and their Electron Diffraction (ED) of $Li_{3-X}V_{2-X}Ti_X(PO_4)_3$/MWCNT composites for X = 0.0(upper) and 0.1(lower). The figure compares those two key features before and after immersion of each sample into hot water (60℃; 47h). After immersion in hot water, the pristine LVP (X=0.0) particles completely disappear and only MWCNTs are observed, moreover no diffraction spots in ED; this indicates that the crystal particles are possibly dissolved. In contrast, for Ti-substituted LVP(X=0.1) particles are observed even after immersion in hot water and diffraction spots are observed also in the ED. In contrast, at X=0.1, LVP particles are observed even after immersion in warm water and diffraction spots are observed even in the ED.

High resolution TEM images of $Li_3V_2(PO_4)_3$ and $Li_{2.9}V_{1.9}Ti_{0.1}(PO_4)_3$.

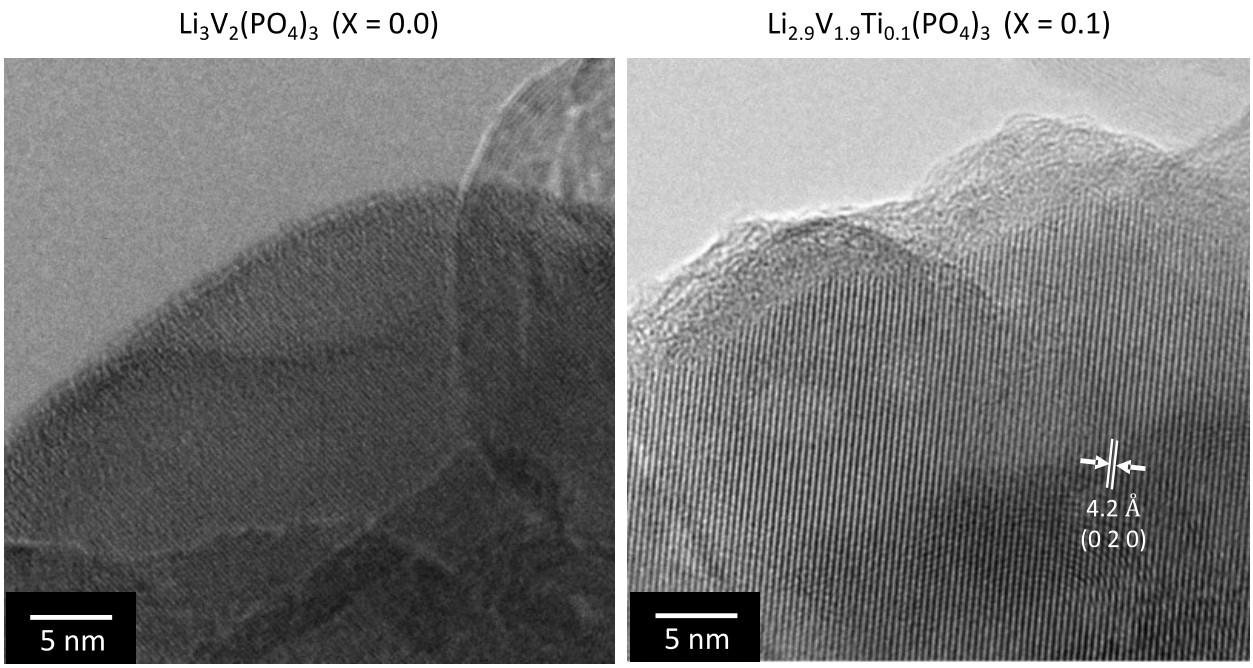

Figure S5. Magnified HRTEM image of $Li_3V_2(PO_4)_3$/MWCNT (right) and $Li_{2.9}V_{1.9}Ti_{0.1}(PO_4)_3$/MWCNT (left) demonstrate a clear crystal lattice aligned along the (020) plane. In addition, an amorphous phase is observed at 2-3 nm on the surface of $Li_{2.9}V_{1.9}Ti_{0.1}(PO_4)_3$/MWCNT.

Composition of $Li_{2.9}V_{1.9}Ti_{0.1}(PO_4)_3$/MWCNTs on the surface and bulk as determined by STEM and EDX.

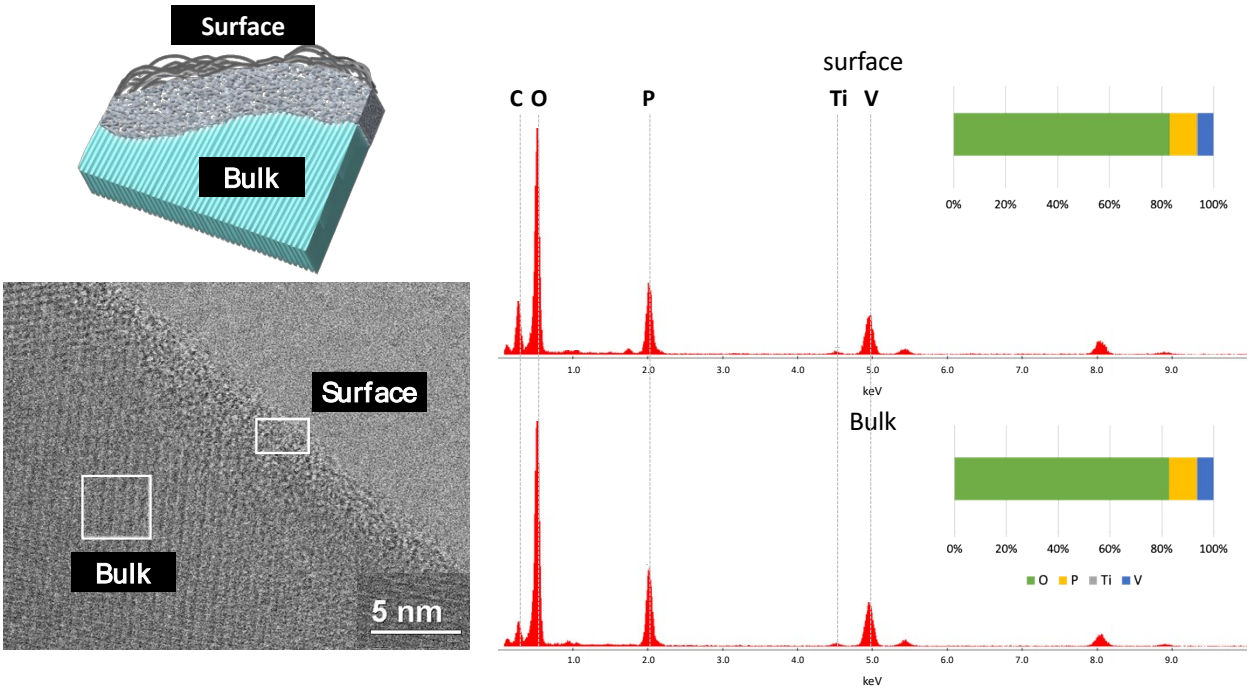

Figure S6. Inside the particle (bulk), lattice pattern corresponding to the face spacing of LVP is observed, and on the surface, an amorphous layer of about 2 nm is observed. EDX of the box shown in the STEM image (corresponding to Surface and Bulk) shows peaks of C, O, P, Ti, and V in each region, all of which are derived from $Li_{2.9}V_{1.9}Ti_{0.1}(PO_4)_3$/MWCNT. In addition, there is no difference in the elemental ratios, indicating that the elemental species and ratio are almost the same on the surface and in the bulks.

Investigation of the degradation states of electrodes after 10,000 cycles full cell cycling of Li//LTO and Li//LVP cells

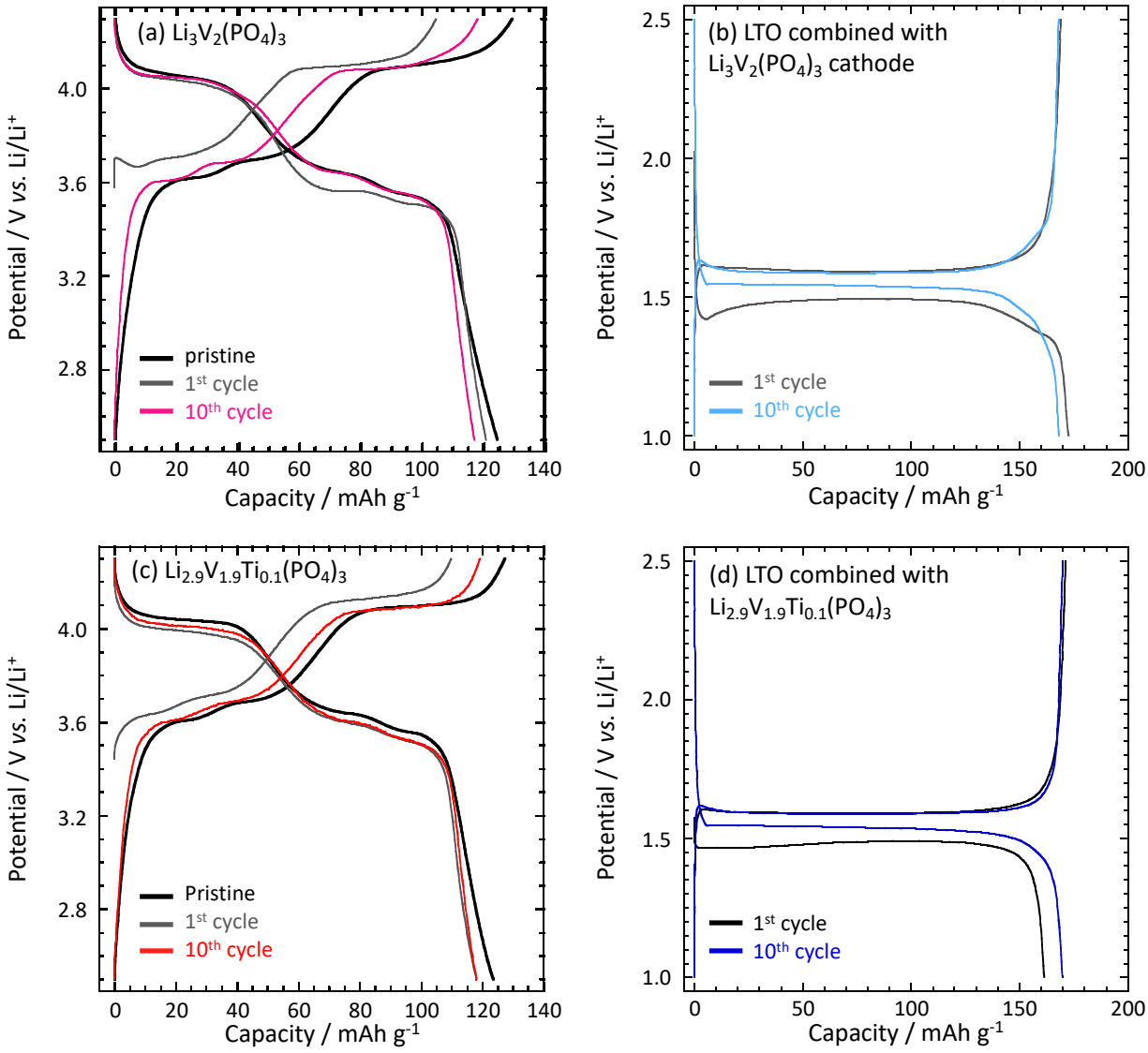

Figure S7. Charge discharge curves of $Li_3V_2(PO_4)_3$, $Li_{2.9}V_{1.9}Ti_{0.1}(PO_4)_3$ and LTO for initial and 10th cycles of Li metal half cells reassembled by using electrodes removed from the full cells after 10,000 cycles: (a) $Li_3V_2(PO_4)_3$ and (b) LTO after 10,000 cycling of full cell without any pretreatment (no preconditioning) and (c) $Li_{2.9}V_{1.9}Ti_{0.1}(PO_4)_3$ and (d) LTO after 10,000 cycling of full cell.

Comparison of Cycle performance of LTO//(Li3-xV2-xTix(PO4)3 (x = 0 and 0.1) full cells at different C-rates

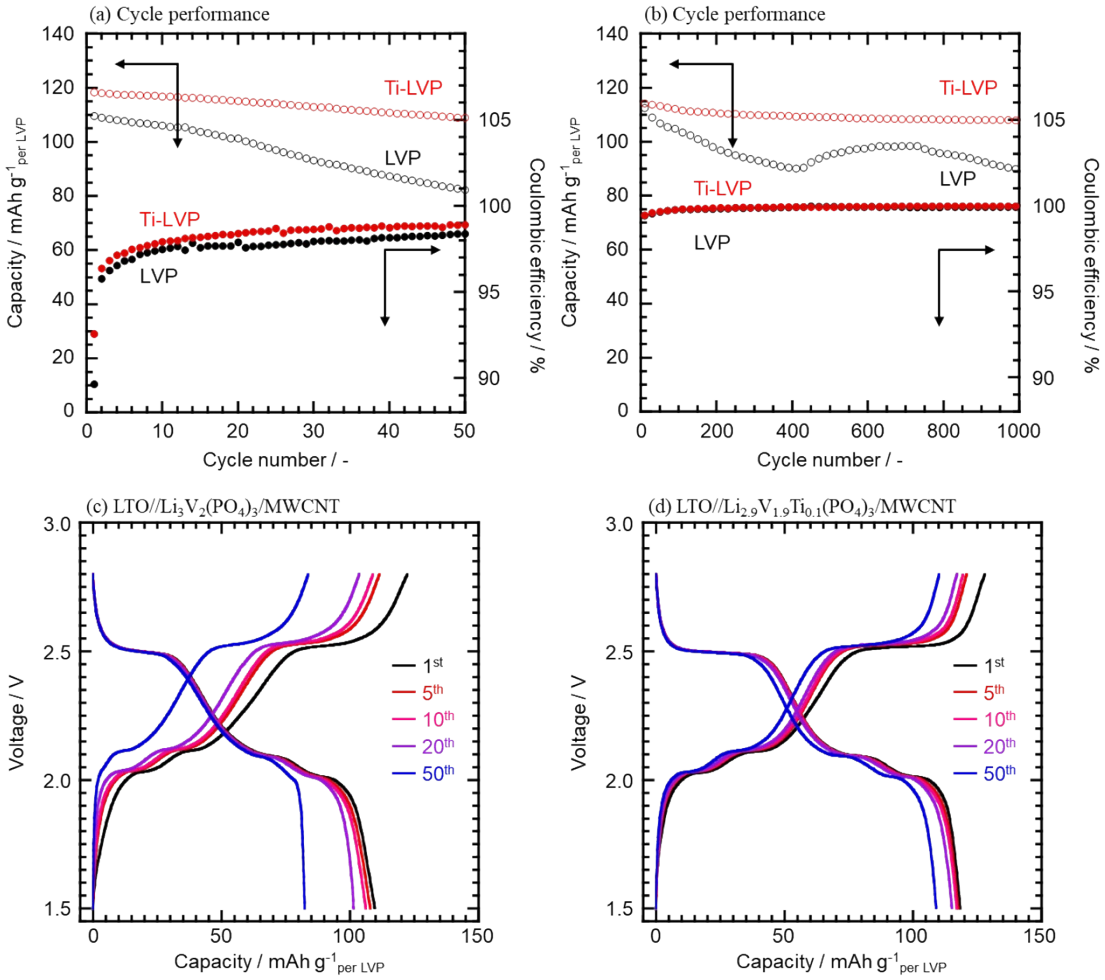

Figure S8. Plots of capacity against the cycle of LTO//($Li_{3-x}V_{2-x}Ti_x(PO_4)_3$(x = 0 and 0.1) full cells. (a) 50 cycles at 0.5C/0.5C rate; (b) 1000 cycles at 10C/10C rate (1C = 131.5 mA $g^{-1}_{per\ LVP}$). Charge discharge curves of (c) LTO//$Li_3V_2(PO_4)_3$ and (d)LTO//$Li_{2.9}V_{1.9}Ti_{0.1}(PO_4)_3$ full-cell at 0.5C-rate. For X = 0.0, the low-potential plateau (0.5Li^+, 2.02 V) decreases continuously, and this plateau almost disappears after 50 cycles. For X = 0.1, there is no marked change in the charge/discharge curve after 50 cycles.

Rate performance of LTO// $Li_3V_2(PO_4)_3$ and LTO// $Li_{2.9}V_{1.9}Ti_{0.1}(PO_4)_3$ full cell

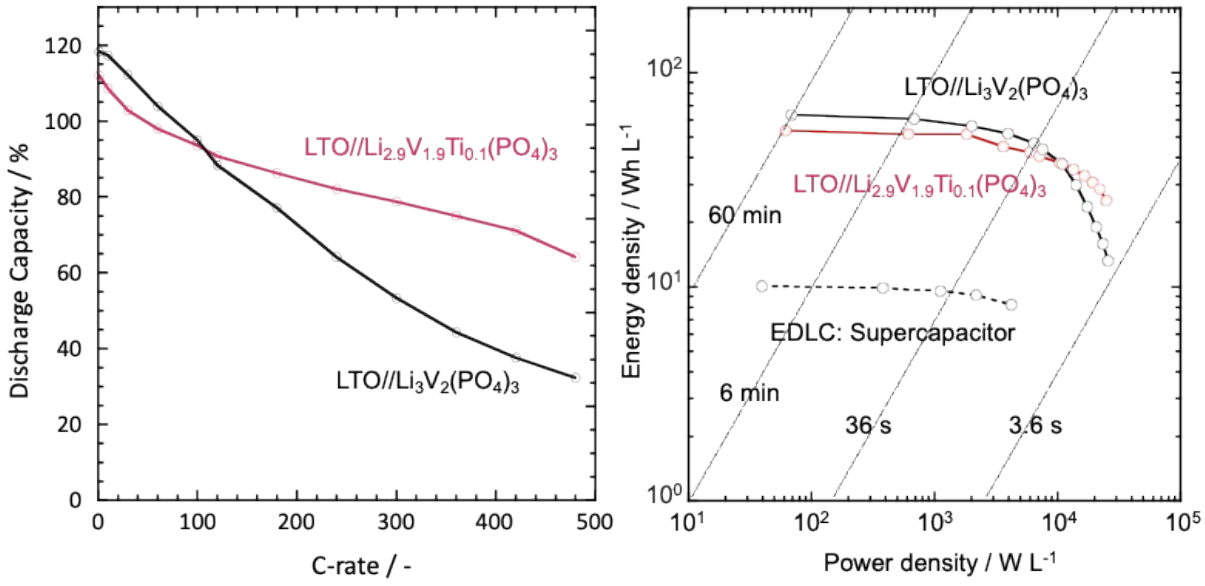

Figure S9. The tested LTO// $Li_{2.9}V_{1.9}Ti_{0.1}(PO_4)_3$ system exhibits excellent discharge C-rate capability (left); 94 mAh g-1 at 100C, and then 79 mAh g^{-1} at 300C, corresponding to the 83 and 70% of the capacity obtained at 1C. Ragone plots of our full cells LTO//$Li_3V_2(PO_4)_3$, LTO//$Li_{2.9}V_{1.9}Ti_{0.1}(PO_4)_3$ and supercapacitor: SC [AC/1 M $TEMABF_4$/PC/AC] (right). All the volumetric capacity was calculated based on toral volume of two electrodes. LTO// $Li_{2.9}V_{1.9}Ti_{0.1}(PO_4)_3$ full cells exhibit high volumetric energy density of 51.4-53.6 Wh L^{-1} within the region of low power requirement (100 – 2,000 W L^{-1}) which corresponds to the 5-folds volumetric energy density of SC.[2] Even at a higher power (2,000 – 25,000 W L^{-1}), 50% of the energy density (25.3-51.6 Wh L^{-1}) can be maintained.

XPS spectra for two different kinds of cathodes($Li_3V_2(PO_4)_3$ and $Li_{2.9}V_{1.9}Ti_{0.1}(PO_4)_3$) and anode($Li_4Ti_5O_{12}$:LTO)

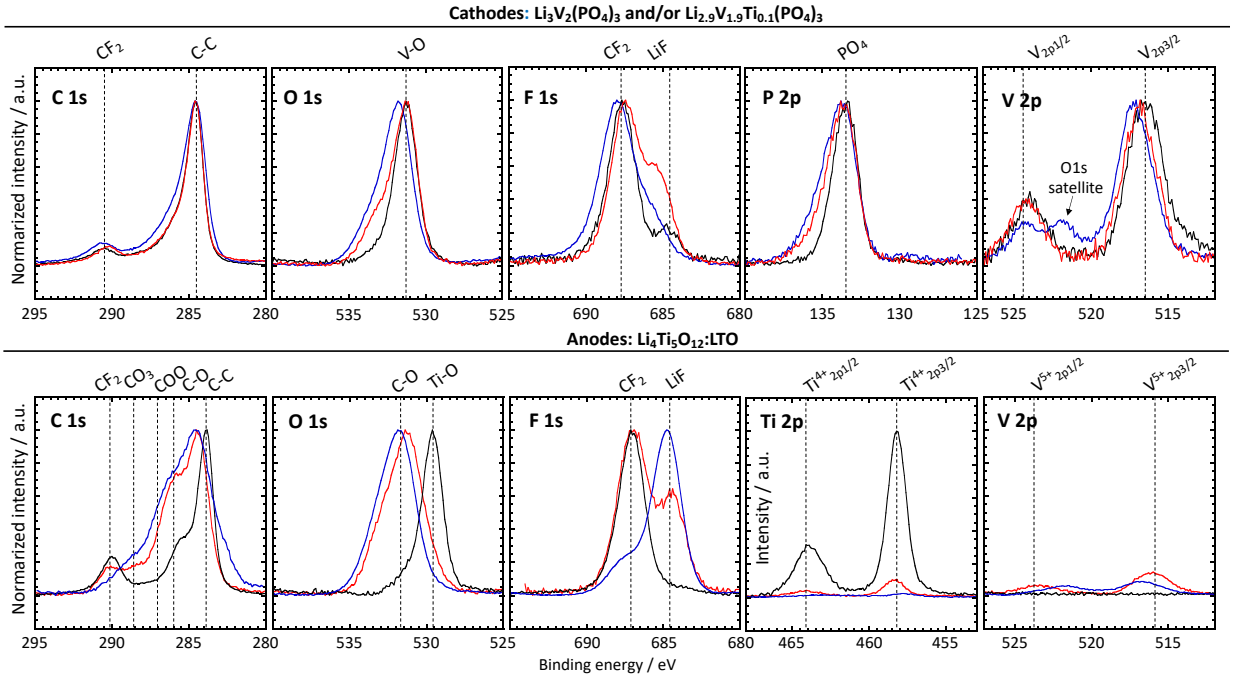

Figure S10. XPS spectra for (upper) two different kinds of cathodes ($Li_3V_2(PO_4)_3$ and $Li_{2.9}V_{1.9}Ti_{0.1}(PO_4)_3$) and (lower) anode ($Li_4Ti_5O_{12}$: LTO). The upper spectra have been obtained in various conditions: (black) is a pristine $Li_{2.9}V_{1.9}Ti_{0.1}(PO_4)_3$ before cycling, (blue) represents $Li_3V_2(PO_4)_3$ after 10,000 cycles and (red) $Li_{2.9}V_{1.9}Ti_{0.1}(PO_4)_3$ after 10,000 cycles. Likewise, the lower spectra show the XPS spectra for anodes (LTO) under different conditions: (black) Pristine LTO, (blue) LTO anode after 10,000 cycles (w/$Li_3V_2(PO_4)_3$ cathode), and (red) LTO anode after 10,000 cycles (w/$Li_{2.9}V_{1.9}Ti_{0.1}(PO_4)_3$ cathode). In Cathode, a peak corresponding to LiF was observed at 684.5 eV in the F 1s spectra of both $Li_3V_2(PO_4)_3$ and $Li_{2.9}V_{1.9}Ti_{0.1}(PO_4)_3$ after 10,000 cycles, indicating that LiF is formed as the electrolyte decomposition. In the spectra of $Li_3V_2(PO_4)_3$ after 10,000 cycles, a peak is observed at 520 eV, but this is considered a satellite peak of O1s detected and is not considered a spectral change due to capacity degradation during cycle. In the anode, peaks corresponding to C-O derived from Li_2CO_3 and $ROCO_2$, which are electrolyte deposition, are observed in the C 1s and O 1s spectra. A peak corresponding to LiF is also observed at 684.5 eV in the F 1s spectra. In the Ti 2p spectra, although the Ti^{4+} 2p 3/2 peak derived from LTO is observed in pristine LTO, its peak completely disappears in the LTO anode after 10,000 cycles (w/$Li_3V_2(PO_4)_3$ cathode), indicating that the LTO is completely covered by deposition. On the other hand, in the LTO anode after 10,000 cycles (w/$Li_{2.9}V_{1.9}Ti_{0.1}(PO_4)_3$ cathode), Ti^{4+} 2p 3/2 peak is still observable, indicating that there are few deposition on the LTO surface. In the V 2p spectra, in both LTO anode after 10,000 cycles (w/$Li_3V_2(PO_4)_3$ cathode) and LTO anode after 10,000 cycles (w/$Li_{2.9}V_{1.9}Ti_{0.1}(PO_4)_3$ cathode), the V^{5+} 2p1/ 2 peak was observed and it is thought that cathode-derived vanadium is deposited, but the peak intensity is so small so that it is hard to discuss the quantitative.

The amount of vanadium dissolved after cycle test measured from the ICP-MS.

Table S3. Results of ICP-MS on vanadium detection among two LTO samples and corresponding electrolytes after 1,000 cycles using $Li_3V_2(PO_4)_3$ and $Li_{2.9}V_{1.9}Ti_{0.1}(PO_4)_3$ as cathode.

Cathode	Vanadium on 5.3-5.8 mg of $Li_4Ti_5O_{12}$		Vanadium in 2,000 µL (1.3 g cm-3) of electrolyte		Total amount of vanadium
	ppm	µg	ppm	µg	µg
$Li_3V_2(PO_4)_3$	630	3.4	0.81	2.1	5.5
$Li_{2.9}V_{1.9}Ti_{0.1}(PO_4)_3$	320	1.9	0.88	2.3	4.1

Reference

1 S.-C. Yin, H. Grondey, P. Strobel, M. Anne and L. F. Nazar, *J. Am. Chem. Soc.*, 2003, **125**, 10402–10411.

2 K. Naoi, W. Naoi, S. Aoyagi, J.-I. Miyamoto and T. Kamino, *Acc. Chem. Res.*, 2013, **46**, 1075–1083.